Nanoscale

RSCPublishing

ARTICLE

Electro-Mechanical Anisotropy of Phosphorene

Cite this: DOI:10.1039/C5NR00355E

Luqing Wang[a], Alex Kutana[a], Xiaolong Zou[a] and Boris I. Yakobson[a,b,c,*],

Received 16th January 2015,
Accepted 17th April 2015

DOI: 10.1039/C5NR00355E

www.rsc.org/

Applied uniaxial stress can break the original symmetry of material, providing an experimentally feasible way to alter material properties. Here, we explore the effects of uniaxial stress along an arbitrary direction on mechanical and electronic properties of phosphorene, showing the enhancement of inherent anisotropy. Basic physical quantities including Young's modulus, Poisson's ratio, band gap, and effective carrier masses under external stress are all computed from the first principles with the density functional theory, while the final results are presented in compact analytical forms.

Keywords: phosphorene, uniaxial stress, band gap, elastic properties, first-principles calculations.

1. Introduction

Following the successful exfoliation and growth of graphene and subsequent synthesis of a large group of other two-dimensional (2D) materials,[1] 2D black phosphorus (P) is a recent addition to the family. [2] Few-nanometer thick micron-size flakes of black phosphorus were fabricated by Li et al.[3] Field effect transistors made from this monoelemental 2D material with direct band gap have displayed attractive characteristics, including room-temperature on/off ratio of 10^5 and a peak field effect mobility near 1000 $cm^2\ V^{-1}\ s^{-1}$, [3, 4] making 2D P a promising candidate for electronic and optoelectronic devices.[5-9] In addition, black phosphorus is unique among layered materials[10-14] due to its significant in-plane anisotropy, which may allow for the realization of novel thin-film infrared polarizers,[15] originating from its C_{2h} symmetry. [16] Arbitrarily directed applied uniaxial stress can break this symmetry and enhance the anisotropy, and thus can then be used for anisotropic modulation of the electronic, magnetic, optical and transport properties, e.g. to vary its anisotropic free-carrier mobility or the preferred conductivity direction. [17] Hence, a systematic exploration of stress-enhanced anisotropy in 2D P (phosphorene) [4] is of great interest. In this work, we study mechanical and electronic response of phosphorene to applied uniaxial stress along an arbitrary direction, and calculate some key parameters, such as Poisson's ratio, Young's modulus, band gap, and effective carrier masses. Uniaxial stress can be experimentally realized in 2D materials through epitaxial lattice mismatch, [18] functional wrapping, [19, 20] doping, [21, 22] and simply applying external tension. [23]

2. Results and discussion

2.1 Computational Methods

The first-principle density functional theory (DFT) calculations were performed using the Vienna Ab initio Simulation Package (VASP). [24] Structural optimization and self-consistent total energy calculations were performed adopting generalized gradient approximation (GGA) with the Perdew-Burke-Ernzerhof (PBE) exchange-correlation functional along with the projector-augmented wave (PAW) potentials. Electronic wave functions were expanded in a plane wave basis set with the kinetic energy cutoff of 400 eV and for the Brillouin zone integration a 15 × 11 × 1 Monkhorst-Pack k-point mesh was used. Besides standard DFT with GGA, hybrid Heyd-Scuseria-Ernzerhof (HSE)06 method[25, 26] was also employed to investigate the electronic properties and obtain an accurate description of electronic states of phosphorene. In HSE06 method, a fraction of the exact screened Hartree-Fock (HF) exchange is incorporated into the PBE exchange using a mixing parameter $\alpha = 0.25$. A 9 × 6 × 1 Monkhorst-Pack k-point mesh was employed in HSE calculations. The energy convergence criterion for electronic wavefunction was set to be 10^{-5} eV. A vacuum layer of about 18 Å (c = 20 Å) was chosen to guarantee no spurious interaction between layers in monolayer simulations using periodic boundary conditions. In band structure calculations, 100 points were collected along each high-symmetry line in reciprocal space.

2.2 Mechanical Anisotropy

Before carrying out electronic structure analysis of phosphorene under uniaxial stress, we explore its linear mechanical and structural response. Phosphorene has a puckered hexagonal structure with grooves formed by two layers of phosphorus atoms. The unit cell of phosphorene is shown in Figure 1 (a) and (b) with the *x* and *y* axes corresponding to the zigzag (along the grooves) and armchair

(perpendicular to the grooves) directions, respectively. Our calculated lattice constants for unstressed phosphorene are a_1 = 3.30 Å, and a_2 = 4.62 Å, consistent with previous theoretical results[17, 27-30]. The uniaxial strain is applied at the angle θ relative to the x axis ($0° < \theta < \pi/2$ with consideration of symmetry). The uniaxially-stressed phosphorene structure depends on the stress direction θ, the corresponding Poisson's ratio $\nu(\theta)$, and strain $\varepsilon(\theta)$. The stress-free rectangular unit cell of phosphorene becomes a rhomboid under applied stress along direction θ as shown in Figure 1 (c).

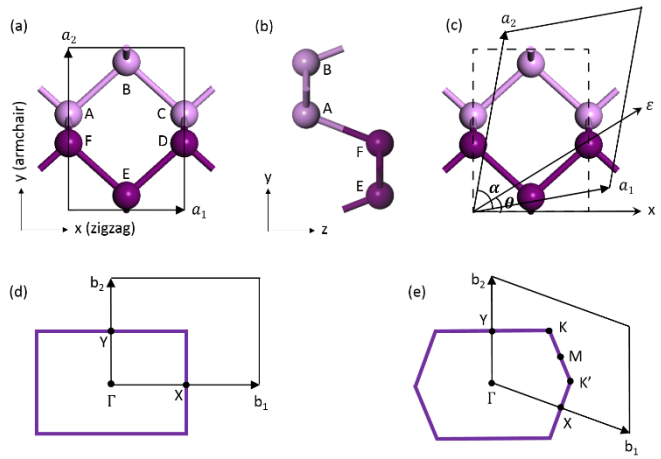

Figure 1. (a) Top and (b) side views of the unstressed phosphorene primitive cell. Atoms in top and bottom layers are shown darker and lighter, respectively. (c) Top view of the phosphorene cell under uniaxial strain defined by direction θ. First Brillouin zone of the (d) unstressed and (e) uniaxially-stressed phosphorene primitive cell.

In a 2D material, an arbitrary stress tensor $\boldsymbol{\sigma}$ and strain tensor $\boldsymbol{\varepsilon}$ can be expressed as 2×2 matrices,

$$\boldsymbol{\sigma} = \begin{bmatrix} \sigma_{xx} & \sigma_{xy} \\ \sigma_{xy} & \sigma_{yy} \end{bmatrix}, \text{ and } \boldsymbol{\varepsilon} = \begin{bmatrix} \varepsilon_{xx} & \varepsilon_{xy} \\ \varepsilon_{xy} & \varepsilon_{yy} \end{bmatrix}.$$

For materials with orthogonal symmetry, their relation under plane stress conditions can be written as:

$$\begin{bmatrix} \sigma_{xx} \\ \sigma_{yy} \\ \sigma_{xy} \end{bmatrix} = \begin{bmatrix} C_{11} & C_{12} & 0 \\ C_{12} & C_{22} & 0 \\ 0 & 0 & C_{66} \end{bmatrix} \begin{bmatrix} \varepsilon_{xx} \\ \varepsilon_{yy} \\ 2\varepsilon_{xy} \end{bmatrix}$$

where Voigt notation has been used for the stiffness tensor C_{ij}. In the coordinate system where the x axis is aligned with the direction of stress, the strain matrix can be written as $\boldsymbol{\varepsilon}'=[(\varepsilon,0),(0,-\varepsilon\nu)]$, where ε is the magnitude of the uniaxial strain and ν is the Poisson's ratio. The strain matrix $\boldsymbol{\varepsilon}$ in the original coordinate system is then obtained as $\boldsymbol{\varepsilon}=\boldsymbol{R}\boldsymbol{\varepsilon}'\boldsymbol{R}^{\mathrm{T}}$ where $\boldsymbol{R}$ is the in-plane rotation matrix. Our results for the components of the stiffness tensor C_{ij} and other elastic properties of phosphorene are summarized in Table 1.

Table 1. The calculated stiffness tensor components, Young's modulus, Poisson's ratio and shear modulus of phosphorene

Unit	Stiffness tensor components				Poisson's ratio		Young's modulus		Shear modulus
	C_{11}	C_{22}	C_{12}	C_{66}	Zigzag	Armchair	Zigzag	Armchair	
GPa·nm	105.2	26.2	18.4	22.4	0.703	0.175	92.3	23.0	22.4

Uniaxial deformation results in compression along the direction that is perpendicular to the direction of applied tension, as described by the material Poisson's ratio. We derived the expression for the Poisson's ratio of phosphorene $\nu(\theta)$ along an arbitrary direction θ (see the Supplemental Information):

$$\nu(\theta) = \frac{(\nu_{zz}cos^4\theta - d_1 cos^2\theta sin^2\theta + \nu_{zz}sin^4\theta)}{(cos^4\theta + d_2 cos^2\theta sin^2\theta + d_3 sin^4\theta)} \quad (1)$$

Here ν_{zz}=0.703 is the Poisson's ratio along the zigzag direction, and d_1=0.894, d_2=2.712, and d_3=4.012. The Poisson's ratio of phosphorene displays nonmonotonic θ dependence, first decreasing and then increasing with θ, as shown in Figure 2 (a). It is highly anisotropic, with a value of 0.703 along the zigzag direction and 0.175 along armchair direction. The minimum Poisson's ratio of 0.064 is achieved around θ = 47.5°.

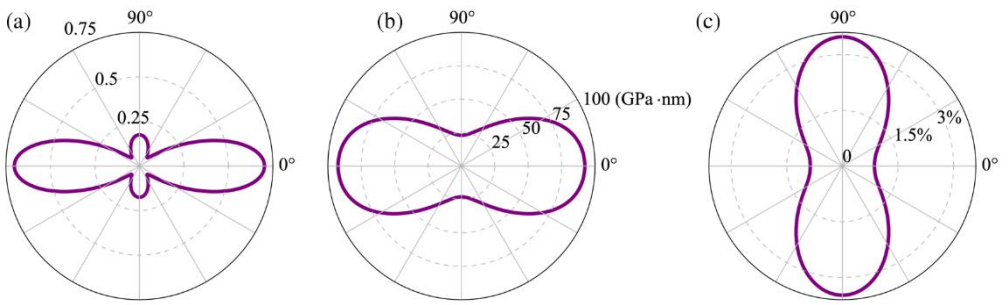

Figure 2. Calculated orientation-dependent (a) Poisson's ratio $\nu(\theta)$, (b) Young's modulus $Y(\theta)$ of phosphorene, and (c) orientation-dependent strain $\varepsilon(\theta)$ in phosphorene corresponding to constant stress σ=0.8GPa·nm.

The orientation-dependent Young's modulus $Y(\theta)$ is defined according to $Y(\theta)=\sigma/\varepsilon(\theta)$, where σ is the orientation-independent constant stress. For phosphorene, the dependence of Young's modulus on the angle θ is given by:

$$Y(\theta) = Y_{zz}/(cos^4\theta + d_2 cos^2\theta sin^2\theta + d_3 sin^4\theta) \quad (2)$$

Here, Y_{zz}=92.3 GPa·nm is the Young's modulus along the zigzag direction, and coefficients d_2 and d_3 are same as in Equation (1). The Young's modulus decreases monotonically from the maximum value of 92.3 GPa·nm along the zigzag direction (θ = 0°) to a minimum value of 23.0 GPa·nm along armchair direction. Derivation of Equation (2) can be found in the Supplemental Info. The obtained full orientation-dependent Young's modulus of phosphorene is plotted in Figure 2 (b).

Due to anisotropy of phosphorene, same stress applied along different directions would result in different strain values. From $\varepsilon=\sigma/Y$, various strains corresponding to constant stress conditions may be obtained. The strains along different directions corresponding to constant stress of σ = 1 GPa·nm can be expressed as:

$$\varepsilon(\theta) = f(cos^4\theta + d_2 cos^2\theta sin^2\theta + d_3 sin^4\theta) \quad (3)$$

where f=1.084%. Figure 2 (c) shows strains along different directions, corresponding to constant stress of σ = 0.8 GPa·nm. This stress results in the strain of 0.87% along the zigzag direction and 3.48% along the armchair direction. The changes of the bond lengths and angles under uniaxial stress σ = 0.8GPa·nm along different directions are summarized in the Supplemental Info. From the engineering point of view, the reversible elastic stress is expected to be most useful. Accordingly, we confine our study to the elastic deformation regime with $\varepsilon < 0.04$. Additionally, it has been reported that a direct-to-indirect transition in the phosphorene band gap occurs at a strain exceeding 0.04, [17, 28] and here we focus on the anisotropy before this transition.

2.3 Electronic Anisotropy

We now turn to the discussion of the electronic structures and the changes it undergoes upon applies tensile stress. The shape of the first Brillouin zone of phosphorene changes from a rectangle to irregular hexagon under uniaxial stress, as shown in Figures 1 (d-e). This shape change can be understood by noting that all the points along the KK' line in uniaxially-stressed phosphorene become a single point in the unstressed material.

Based on the relaxed configurations obtained, we compare the band structures of the unstressed and uniaxially-stressed phosphorene. The band structures of phosphorene under uniaxial stress of σ = 0.8 GPa·nm along different directions are shown in Figure 3, exhibiting direct band gap at the Γ point in all cases. In the unstressed phosphorene, the obtained PBE band gap is 0.89 eV. While the GGA (or LDA) functionals systematically underestimate band gaps, it has been shown that they yield correct slopes for linear deformations in phosphorene [28, 31] and other 2D materials. [32] Our computed HSE06 band gap of unstressed phosphorene is 1.60 eV which agrees well with other theoretical works[27, 28, 30]. Most likely, this value still underestimates the single-particle gap, considering the reported[4] experimental optical gap of 1.45 eV and taking into account an extremely large (0.8 eV) exciton binding energy[31] in this material.

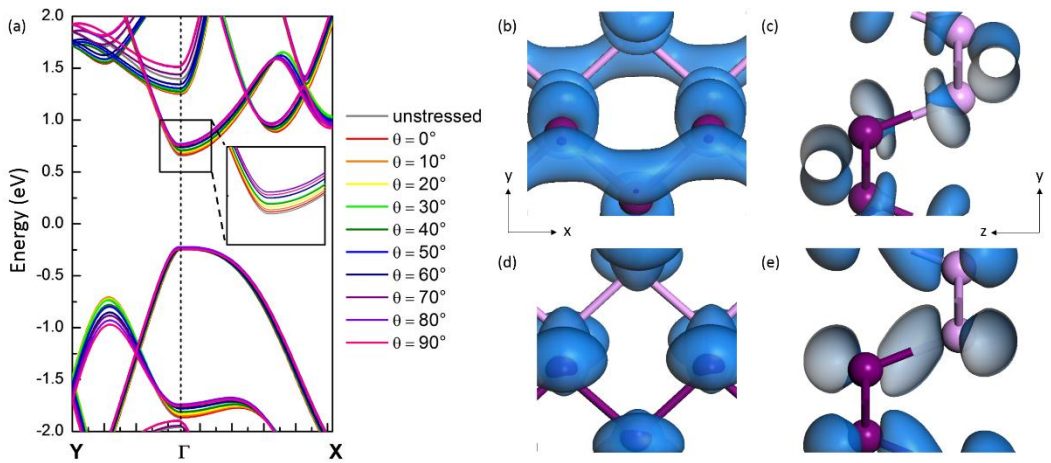

Figure 3. (a) Band structure of unstressed and various directional uniaxial-stressed phosphorene. Electron density isosurface plots of (b) top- and (c) side-views for CBM, and (d) top- and (e) side-views for VBM of phosphorene under uniaxial stress along θ = 40°.

Under applied stress, the position of the valence band maximum (VBM) changes very little, while the conduction band minimum (CBM) moves up, increasing the band gap. The analysis of electron density isosurface plots shows that uniaxial stress does not change the character of electron density distribution at the CBM and VBM appreciably within the elastic deformation regime. The orbital plots of CBM and VBM for stress applied along θ = 40° are shown in Figures 3 (b-e). At CBM, in-plane atoms form bonds and there is no binding for interlayer atoms; whereas at VBM, in-plane atoms do not bind while there are anti-bonding orbitals between interlayer atoms.

Figure 4 shows the PBE band gap of phosphorene under the uniaxial in-plane stress in various directions. Different band gap values along different uniaxial stress directions further demonstrate the anisotropy of phosphorene. The band gap increases with increasing θ, with the minimum value of 0.91 eV along zigzag direction and the maximum value of 1.00 eV along armchair direction. The effect of stress in phosphorene is opposite in direction to transition metal dichalcogenides where the gap decreases with stress [32, 33]. The band gap is most sensitive to the stress applied in the armchair direction. We describe this anisotropy of band gap under constant stress for monolayer phosphorene with the following expression:

$$E_g(\theta,\sigma) = E_g(\theta,0) + \sigma(\, h_1 cos^2\theta + h_2 cos\theta sin\theta + h_3 sin^2\theta) \quad (4)$$

where θ is stress direction and σ is applied stress, $E_g(\theta,0)$ = 0.89 eV, h_1 = 0.0250 eV /(GPa·nm), h_2 = 0.0125 eV/(GPa·nm), h_3 = 0.1375 eV/(GPa·nm). The three independent components of the stress tensor ($\cos^2\theta$, $\cos\theta \sin\theta$, and $\sin^2\theta$) are used as expansion factors. HSE06 method gives consistently larger values for the band gaps of phosphorene under uniaxial in-plane stress, but similar results of the stress effects on the band gap, compared with PBE method. The HSE06 band gap can be found in Figure S1 of the Supplemental Information. Based on HSE06, the minimum and maximum values are found to be 1.62 eV and 1.71 eV with stress along zigzag and armchair directions, respectively. HSE06 results share the same expression form with PBE as Equation (4), while the parameters change to $E_g(\theta,0)$ = 1.60 eV, h_1 = 0.0341 eV /(GPa·nm), h_2 = 0.0220 eV/(GPa·nm), h_3 = 0.1386 eV/(GPa·nm). The HSE06 band gap of phosphorene under the uniaxial in-plane stress in various directions is provided in Figure S1of the Supplemental Information. The main difference with the PBE is that an almost constant shift is added to the fitting line for the HSE06.

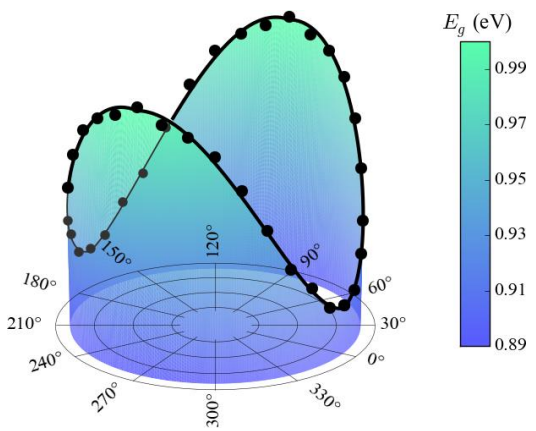

Figure 4. Computed band gap values and fitting line for monolayer phosphorene uniaxially stressed in-plane along different directions, at σ=0.8 GPa·nm. The base value of 0.89 eV represents the gap for unstrained material.

The anisotropic structure results in the direction-dependent effective carrier masses, even without applied stress. Based on the quadratic *E-k* dispersion relationship near the CBM and VBM, we derived the expression for the direction-dependent effective carrier mass m^* of phosphorene as:

$$m^* = 1/(cos^2\varphi/m_{zz}^* + sin^2\varphi/m_{ac}^*) \quad (5)$$

where $0 \le \varphi < 2\pi$ is the angle between an arbitrary direction and the positive *x* axis, and the coefficients m_{zz}^* and m_{ac}^* are the effective carrier masses along zigzag and armchair directions, respectively. In order to study whether and how the uniaxial stress affects the direction-dependent effective carrier mass in phosphorene, we compared the effective masses in unstressed and stressed phosphorene with the uniaxial stress applied along different selected directions θ. Under these conditions, coefficients m_{zz}^* and m_{ac}^* in Equation (5) depend on angle θ. The effective masses of carriers m^* were calculated by parabolic fitting of band extrema according to $E = \hbar^2k^2/2m^*$. A *k*-point spacing of 0.025 Å^{-1} was used. The direction-dependent PBE effective carrier masses (m^*) are plotted in Figure 5 for different stress directions. The PBE coefficients m_{zz}^* and m_{ac}^* corresponding to various stress directions θ are listed in Table 2 for both electrons and holes. Computed effective carrier masses based on HSE06 show similar trends. The HSE06 effective carrier masses (m^*) and coefficients m_{zz}^* and m_{ac}^* can be found in Figure S2 of the Supplemental Information and Table 2 in main text.

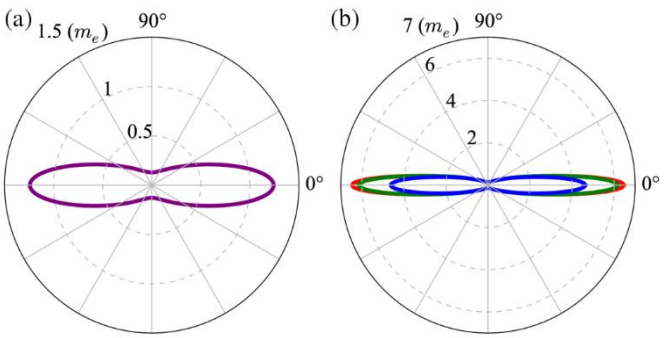

Figure 5. Effective masses of (a) electrons and (b) holes in phosphorene under uniaxial stress 0.8 GPa·nm along different directions. For electrons, the effective mass remains nearly unchanged with stress (purple line). For holes, effective mass is sensitive to stress and its direction θ, as shown for unstressed phosphorene (red), and phosphorene with stress of applied along θ = 0° (green), and θ = 90° (blue).

Table 2. Coefficients for the expression for effective carrier masses in phosphorene for stresses 0.8 GPa·nm applied along various directions as Equation (5).

Coefficient		Electrons	Holes		
			Unstressed	θ = 0°	θ = 90°
m^*_{zz}	PBE	1.242	6.475	6.160	4.629
	HSE06	1.118	6.372	5.448	4.574
m^*_{ac}	PBE	0.128	0.121	0.127	0.127
	HSE06	0.170	0.155	0.161	0.157

Uniaxial stress does not change the effective mass of electrons significantly, whereas the hole effective mass is sensitive to stress. Our calculated PBE electron effective mass is $1.242m_e$ along zigzag direction and $0.128m_e$ along armchair direction, where m_e is the mass of free electron in vacuum, yielding a mass anisotropy of more than 9 times. The hole effective mass is $6.475m_e$ along zigzag direction and $0.121m_e$ along armchair direction (an anisotropy of ~54), in agreement with previous works[17, 27]. Under uniaxial stress, the hole effective mass along zigzag direction decreases significantly, while that along armchair direction remains almost unchanged. The hole mass is most sensitive to constant stress along the armchair direction. Under the constant stress of 0.8 GPa·nm along the zigzag direction, the hole effective mass is $6.160m_e$ along zigzag direction and $0.127m_e$ along armchair direction; under same constant stress along the armchair direction, the hole mass is $4.629m_e$ and $0.127m_e$ along the zigzag and armchair directions, respectively. Based on HSE06 method, electron effective mass is $1.118m_e$ along zigzag direction and $0.170m_e$ along armchair direction, while hole effective mass is 6.372 m_e along zigzag direction and 0.155 m_e along armchair direction (See Figure S2 of the Supplemental Information and Table 2 in main text). HSE06 also predicts that the hole mass is most sensitive to constant stress along the armchair direction. Under the constant stress of 0.8 GPa·nm along the zigzag direction, the HSE06 hole effective mass is $6.013m_e$ along zigzag direction and $0.163m_e$ along armchair direction; under same constant stress along the armchair direction, the hole mass is $4.574m_e$ and $0.157m_e$ along the zigzag and armchair directions, respectively.

Under elastic deformation, the band gap of phosphorene varies depending on the directions of stress. This should generally have interesting manifestations in the polycrystalline phosphorene response to applied tensile load, when differently oriented monocrystal-domains would thus acquire different band gaps. Based on the properties explored above, we illustrate it here with one specific phosphorene-based hetero-junction. Following previous analysis for graphene (see Figure 2e in Ref. [34]) we design the ZZ|AC grain boundary (GB) in a similar way for phosphorene: Figure 6 shows a junction made from two semi-infinite phosphorene sheets with their in-plane crystal orientations rotated by 90° with respect to each other after structural relaxation, with a characteristic GB along the interface edge.[30] The grains on both sides of the boundary have the same band gap without stress; however, after application of stress perpendicular to the grain boundary, as shown in Figure 6, the gaps on the two sides of the boundary become different. If voltage is applied in the same direction, stress can be used to control the switching properties of the junction. A detailed study of electronic properties of the phosphorene hetero-junctions thus can be of interest although it is beyond the scope of present study.

The electro-mechanical anisotropy of phosphorene results from its in-plane anisotropic structure, in which zigzag is the most rigid while armchair is the softest direction. In multi-layer phosphorene, the stacking pattern is such that the zigzag and armchair directions of individual layers are aligned, and thus the two principle directions of anisotropy are preserved. It is thus expected that the uniaxial stress in the few-layer phosphorene will show similar anisotropic trend in its electro-mechanical properties as that of a monolayer. Our computed PBE results for Young's modulus of monolayer phosphorene along zigzag and armchair directions are 92.3 GPa·nm and 23.0 GPa·nm, respectively. In order to compare Young's moduli of monolayer phosphorene and bulk phosphorus, the values for the monolayer are converted into 163.8 GPa and 40.8GPa for the bulk, considering that the effective thickness of the monolayer is 0.5634nm. Based on our PBE calculations for bulk, the Young's moduli along zigzag and armchair directions are 166.3 GPa and 37.8 GPa, respectively. We can see that Young's modulus does not change appreciably from monolayer to bulk, and thus few-layer phosphorene is expected to have a similar Young's modulus. The derivation of the expression for the bulk phosphorene can be found in S7 of the Supplemental Information. Our computed PBE result for the band gap of a monolayer phosphorene is 0.89 eV, and it has been reported that the PBE band gap of bulk phosphorus is 0.33 eV.[35] In the few-layer phosphorene, it is expected that the band gap will decrease monotonically to its bulk value as the number of layers increases.

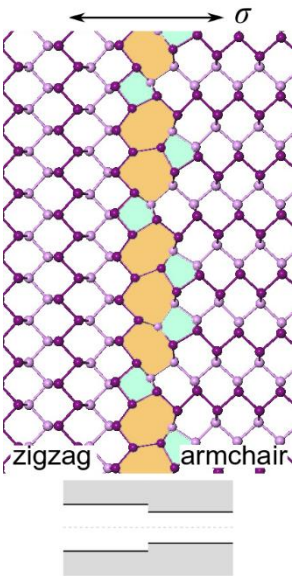

Figure 6. A P-P lateral heterojunction with a grain boundary created by joining two phosphorene sheets rotated by 90° with respect to each other. Atoms in top and bottom layers are shown as dark and light, respectively. The inset shows band alignment of the domains with zigzag and armchair edges after application of stress.

3. Conclusions

In conclusion, we studied the effect of uniaxial stress on the electronic and mechanical properties of phosphorene. The in-plane Poisson's ratio was found to vary nonmonotonically with the

direction of applied stress, passing through a minimum at an angle ~47.5° relative to the zigzag direction. At the same time, Young's modulus decreases monotonically between the zigzag to armchair directions, and the strain produced by constant stress increases. Several geometric parameters of the unit cell change nonmonotonically with the stress direction. Phosphorene preserves its direct gap character with varying stress direction, and the gap increases as the direction of stress is changed from zigzag to armchair. Anisotropic effective carrier masses respond differently to the change in the direction and magnitude of stress. While masses of electrons are largely insensitive to change in the stress direction, hole masses show much greater sensitivity, in particular along the zigzag direction of transport. Anisotropy of phosphorene stress response can be potentially utilized in new devices, such as the proposed electro-mechanical junction constructed from the zigzag-armchair grain boundary.

Supporting Information

S1. Poisson's ratio for monolayer

The unit stress tensor along θ direction is

$$\boldsymbol{\sigma} = \begin{bmatrix}\sigma_{xx} & \sigma_{xy}\\ \sigma_{xy} & \sigma_{yy}\end{bmatrix} = \begin{bmatrix} cos^2\theta & cos\theta sin\theta \\ cos\theta sin\theta & sin^2\theta\end{bmatrix}$$

The relationship between $\boldsymbol{\sigma}$ and the corresponding strain tensor $\boldsymbol{\varepsilon} = \begin{bmatrix}\varepsilon_{xx} & \varepsilon_{xy}\\ \varepsilon_{xy} & \varepsilon_{yy}\end{bmatrix}$ can be described as the stiffness tensor **C**, and for orthogonal symmetry under plane stress conditions is

$$\begin{bmatrix}\sigma_{xx}\\ \sigma_{yy}\\ \sigma_{xy}\end{bmatrix} = \begin{bmatrix}C_{11} & C_{12} & 0\\ C_{21} & C_{22} & 0\\ 0 & 0 & C_{66}\end{bmatrix}\begin{bmatrix}\varepsilon_{xx}\\ \varepsilon_{yy}\\ 2\varepsilon_{xy}\end{bmatrix}$$

The unit vector along θ direction is $\vec{\boldsymbol{\imath}} = \begin{bmatrix}cos\theta\\ sin\theta\end{bmatrix}$ and the unit vector perpendicular to it is $\vec{\boldsymbol{\jmath}} = \begin{bmatrix}-sin\theta\\ cos\theta\end{bmatrix}$

The strain along θ direction corresponding to unit stress is

$$\varepsilon_{\parallel} = \vec{\imath}^T\varepsilon\vec{\imath} = [cos\theta \quad sin\theta]\begin{bmatrix}\varepsilon_{xx} & \varepsilon_{xy}\\ \varepsilon_{xy} & \varepsilon_{yy}\end{bmatrix}\begin{bmatrix}cos\theta\\ sin\theta\end{bmatrix}$$

$$= \frac{C_{22}cos^4\theta - (C_{12}+C_{21})cos^2\theta sin^2\theta + C_{11}sin^4\theta}{C_{11}C_{22}-C_{12}C_{21}} + \frac{cos^2\theta sin^2\theta}{C_{66}}$$

$$= \frac{C_{22}cos^4\theta - 2C_{12}cos^2\theta sin^2\theta + C_{11}sin^4\theta}{C_{11}C_{22}-C_{12}^2} + \frac{cos^2\theta sin^2\theta}{C_{66}}$$

The strain perpendicular to θ direction corresponding to unit stress is

$$\varepsilon_{\perp} = \vec{\jmath}^T\varepsilon\vec{\jmath} = [-sin\theta \quad cos\theta]\begin{bmatrix}\varepsilon_{xx} & \varepsilon_{xy}\\ \varepsilon_{xy} & \varepsilon_{yy}\end{bmatrix}\begin{bmatrix}-sin\theta\\ cos\theta\end{bmatrix}$$

$$= \frac{-C_{21}cos^4\theta + (C_{11}+C_{22})cos^2\theta sin^2\theta - C_{12}sin^4\theta}{C_{11}C_{22}-C_{12}C_{21}} + \frac{-cos^2\theta sin^2\theta}{C_{66}}$$

Poisson's ratio $\nu = -\varepsilon_{\perp}/\varepsilon_{\parallel}$

$$= \frac{\frac{-C_{21}cos^4\theta + (C_{11}+C_{22})cos^2\theta sin^2\theta - C_{12}sin^4\theta}{C_{11}C_{22}-C_{12}C_{21}} + \frac{-cos^2\theta sin^2\theta}{C_{66}}}{\frac{C_{22}cos^4\theta - 2C_{12}cos^2\theta sin^2\theta + C_{11}sin^4\theta}{C_{11}C_{22}-C_{12}^2} + \frac{cos^2\theta sin^2\theta}{C_{66}}}$$

$$= \frac{C_{12}cos^4\theta - \left(C_{11}+C_{22}-\frac{C_{11}C_{22}-C_{12}^2}{C_{66}}\right)cos^2\theta sin^2\theta + C_{12}sin^4\theta}{C_{22}cos^4\theta - (2C_{12}-\frac{C_{11}C_{22}-C_{12}^2}{C_{66}})cos^2\theta sin^2\theta + C_{11}sin^4\theta}$$

In main text Equation (1),

$$\nu_{zz} = \frac{C_{12}}{C_{22}}$$

$$d_1 = \frac{C_{11}}{C_{22}} + 1 - \frac{C_{11}C_{22}-C_{12}^2}{C_{22}C_{66}}$$

$$d_2 = -\left(2\frac{C_{12}}{C_{22}} - \frac{C_{11}C_{22}-C_{12}^2}{C_{22}C_{66}}\right)$$

$$d_3 = \frac{C_{11}}{C_{22}}$$

S2. Young's modulus for monolayer

The unit stress tensor along θ direction

$$\boldsymbol{\sigma} = \begin{bmatrix}\sigma_{xx} & \sigma_{xy}\\ \sigma_{xy} & \sigma_{yy}\end{bmatrix} = \begin{bmatrix} cos^2\theta & cos\theta sin\theta \\ cos\theta sin\theta & sin^2\theta\end{bmatrix}$$

The unit vector along θ direction $\vec{\boldsymbol{\imath}} = \begin{bmatrix}cos\theta\\ sin\theta\end{bmatrix}$ and the unit vector perpendicular to it $\vec{\boldsymbol{\jmath}} = \begin{bmatrix}-sin\theta\\ cos\theta\end{bmatrix}$

The strain along θ direction corresponding to unit stress is

$$\varepsilon_{\parallel} = \vec{\imath}^T\varepsilon\vec{\imath} = [cos\theta \quad sin\theta]\begin{bmatrix}\varepsilon_{xx} & \varepsilon_{xy}\\ \varepsilon_{xy} & \varepsilon_{yy}\end{bmatrix}\begin{bmatrix}cos\theta\\ sin\theta\end{bmatrix}$$

$$= \frac{C_{22}cos^4\theta - (C_{12}+C_{21})cos^2\theta sin^2\theta + C_{11}sin^4\theta}{C_{11}C_{22}-C_{12}C_{21}} + \frac{cos^2\theta sin^2\theta}{C_{66}}$$

$$= \frac{C_{22}cos^4\theta - 2C_{12}cos^2\theta sin^2\theta + C_{11}sin^4\theta}{C_{11}C_{22}-C_{12}^2} + \frac{cos^2\theta sin^2\theta}{C_{66}}$$

Young's modulus $Y = \sigma/\varepsilon_{\parallel}$

$$= \frac{1}{\frac{C_{22}cos^4\theta - 2C_{12}cos^2\theta sin^2\theta + C_{11}sin^4\theta}{C_{11}C_{22}-C_{12}^2} + \frac{cos^2\theta sin^2\theta}{C_{66}}}$$

In main text Equation (2),

$$Y_{zz} = (C_{11}C_{22}-C_{12}^2)/C_{22}$$

S3. Strain corresponding to equivalent stress 1 GPa·nm

$$\varepsilon = \frac{\sigma}{Y} = 1\ \text{GPa}\cdot\text{nm}\cdot\left(\frac{C_{22}cos^4\theta - 2C_{12}cos^2\theta sin^2\theta + C_{11}sin^4\theta}{C_{11}C_{22} - C_{12}^2} + \frac{cos^2\theta sin^2\theta}{C_{66}}\right)$$

In main text Equation (3),

$$f = 1\ \text{GPa}\cdot\text{nm}\cdot\frac{C_{22}}{C_{11}C_{22} - C_{12}^2}$$

S4. Bond lengths and angles of uniaxially-stressed phosphorene

Bond lengths and angles of deformed phosphorene under uniaxial stress σ = 0.8GPa·nm along different directions are summarized in Table S1. Bonds and angles are labeled according to participating atoms. For example, r_{AB} is the bond lengths between atoms A and B, while bond angle ∠ABC is the angle between bonds AB and BC. Bond lengths r_{AB}, r_{BC}, r_{CD}, bond angles ∠ABC, ∠BCD, ∠CDE and the angle between the two primitive vectors α, are shown in Figure 1 (a-c). In unstressed phosphorene, r_{AB} = r_{BC}, and ∠BCD = ∠CDE. After symmetry is broken by the application of uniaxial stress, these bonds and angles are no longer equal. Under the constant stress conditions with the angle θ changing from 0° to 90°, several geometric parameters show nonmonotonic behavior. For instance, ∠BCD decreases first and then increases, and so does angle α. The bond length r_{AB} and angle ∠CDE have the opposite trend – they increase first and then decrease.

Table S1. Bond lengths and bond angles in the unstressed phosphorene and phosphorene under constant uniaxial stress σ=0.8GPa·nm. The numbers in parentheses give fractional changes of the values in each column at θ = 0° and θ = 90° with respect to the unstressed case.

θ(°)	a_1(Å)	a_2(Å)	α(°)	r_{AB}(Å)	r_{BC}(Å)	r_{CD}(Å)	$\angle ABC$(°)	$\angle BCD$(°)	$\angle CDE$(°)
Unstressed	3.300	4.623	90.00	2.222	2.222	2.259	95.93	104.14	104.14
0	3.329	4.595	90.00	2.229	2.229	2.257	96.58	103.89	103.89
	(0.9%)	(-0.6%)		(0.3%)	(0.3%)	(-0.1%)	(0.7%)	(-0.2%)	(-0.2%)
10	3.328	4.600	89.72	2.229	2.228	2.258	96.59	103.77	104.17
20	3.327	4.612	89.50	2.229	2.227	2.257	96.57	103.68	104.41
30	3.326	4.628	89.32	2.231	2.227	2.258	96.53	103.66	104.60
40	3.327	4.648	89.11	2.232	2.226	2.258	96.53	103.63	104.87
50	3.324	4.673	88.86	2.232	2.225	2.261	96.45	103.72	105.31
60	3.315	4.706	88.68	2.230	2.223	2.262	96.23	103.87	105.72
70	3.300	4.742	88.77	2.226	2.219	2.264	95.88	104.24	105.98
80	3.286	4.772	89.25	2.221	2.217	2.266	95.55	104.84	105.92
90	3.280	4.784	90.00	2.217	2.217	2.266	95.44	105.51	105.51
	(-0.6%)	(3.5%)		(-0.2%)	(-0.2%)	(0.3%)	(-0.5%)	(1.3%)	(1.3%)

S5. Band gap

The stress tensor is $\boldsymbol{\sigma} = \begin{bmatrix}\sigma_{xx} & \sigma_{xy}\\ \sigma_{xy} & \sigma_{yy}\end{bmatrix}$ and the strain tensor is $\boldsymbol{\varepsilon} = \begin{bmatrix}\varepsilon_{xx} & \varepsilon_{xy}\\ \varepsilon_{xy} & \varepsilon_{yy}\end{bmatrix}$

Band gap and strain has linear relationship as

$$E_g(\theta,\sigma) = E_g(\theta,0) + A\varepsilon_{xx} + B\varepsilon_{xy} + C\varepsilon_{yy} \quad \text{(S1)}$$

Here, ε_{xx}, ε_{xy}, and ε_{yy} are components of the strain tensor in non-rotated system, aligned with the lattice vectors of the 2D crystal.

Rotation matrix to transform from rotated to non-rotated system is $\boldsymbol{R} = \begin{bmatrix} cos\theta & -sin\theta \\ sin\theta & cos\theta \end{bmatrix}$

For uniaxial stress $\boldsymbol{\sigma'} = \begin{bmatrix} \sigma & 0 \\ 0 & 0 \end{bmatrix}$ along the x' axis in a system rotated counterclockwise by an angle θ w.r.t. non-rotated one, the corresponding stress tensor σ in non-rotated system is given by:

$$\boldsymbol{\sigma} = \boldsymbol{R\sigma' R^T} = \begin{bmatrix} \sigma_{xx} & \sigma_{xy} \\ \sigma_{xy} & \sigma_{yy} \end{bmatrix}$$

$$= \begin{bmatrix} cos\theta & -sin\theta \\ sin\theta & cos\theta \end{bmatrix} \begin{bmatrix} \sigma & 0 \\ 0 & 0 \end{bmatrix} \begin{bmatrix} cos\theta & sin\theta \\ -sin\theta & cos\theta \end{bmatrix}$$

$$= \begin{bmatrix} cos^2\theta & cos\theta sin\theta \\ cos\theta sin\theta & sin^2\theta \end{bmatrix} \sigma$$

In non-rotated system, the relationship between stress and strain is

$$\begin{bmatrix} \sigma_{xx} \\ \sigma_{yy} \\ \sigma_{xy} \end{bmatrix} = \begin{bmatrix} C_{11} & C_{12} & 0 \\ C_{12} & C_{22} & 0 \\ 0 & 0 & C_{66} \end{bmatrix} \begin{bmatrix} \varepsilon_{xx} \\ \varepsilon_{yy} \\ 2\varepsilon_{xy} \end{bmatrix}$$

$$\begin{cases} \varepsilon_{xx} = \frac{C_{22}\sigma_{xx} - C_{12}\sigma_{yy}}{C_{11}C_{22} - C_{12}^2} = \frac{C_{22}cos^2\theta - C_{12}sin^2\theta}{C_{11}C_{22} - C_{12}^2}\sigma \\ \varepsilon_{yy} = \frac{C_{11}\sigma_{yy} - C_{12}\sigma_{xx}}{C_{11}C_{22} - C_{12}^2} = \frac{C_{11}sin^2\theta - C_{12}cos^2\theta}{C_{11}C_{22} - C_{12}^2}\sigma \\ \varepsilon_{xy} = \frac{\sigma_{xy}}{2C_{66}} = \frac{cos\theta sin\theta}{2C_{66}}\sigma \end{cases}$$

(S2)

Substituting Equation (S2) into Equation (S1), we can get the band gap of phosphorene under uniaxial stress σ applied along arbitrary direction θ:

$$E_g(\theta,\sigma) = E_g(\theta,0) + A\frac{C_{22}cos^2\theta - C_{12}sin^2\theta}{C_{11}C_{22} - C_{12}^2}\sigma + B\frac{cos\theta sin\theta}{2C_{66}}\sigma + C\frac{C_{11}sin^2\theta - C_{12}cos^2\theta}{C_{11}C_{22} - C_{12}^2}\sigma$$

$$= E_g(\theta,0) + (\frac{AC_{22} - CC_{12}}{C_{11}C_{22} - C_{12}^2}cos^2\theta + \frac{B}{2C_{66}}cos\theta sin\theta + \frac{CC_{11} - AC_{12}}{C_{11}C_{22} - C_{12}^2}sin^2\theta)\sigma$$

$$= E_g(\theta,0) + \sigma(\, h_1cos^2\theta + h_2cos\theta sin\theta + h_3sin^2\theta)$$

Three parameters h_1, h_2, h_3 can be got by fitting results from DFT calculation.

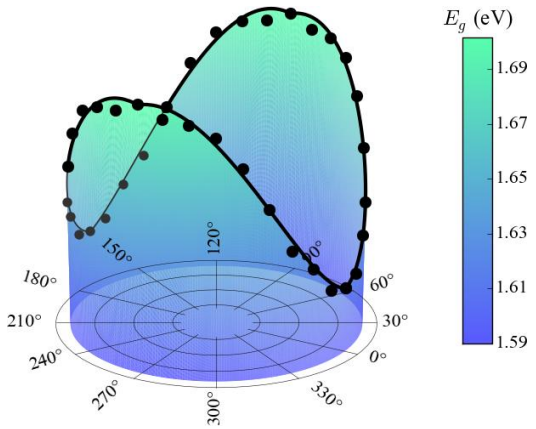

Figure S1. Computed band gap values based on HSE06 method and fitting line for monolayer phosphorene uniaxially stressed in-plane along different directions, at σ=0.8 GPa·nm. The base value of 1.60 eV represents the gap for unstrained material.

S6. Effective mass

Based on the quadratic $E = \frac{\hbar^2 k^2}{2m}$ dispersion relationship, the energy surface near the CBM and VBM can be described as elliptic parabolic surface equation:

$$E = ak_x^2 + bk_y^2 = ak^2cos^2\theta + bk^2sin^2\theta$$

and its second derivative is $\frac{\partial^2 E}{\partial k^2} = 2acos^2\theta + 2bsin^2\theta$.

The effective mass is related with the second derivative of energy:

$$m^* = \frac{\hbar^2}{\frac{\partial^2 E}{\partial k^2}} = \frac{\hbar^2}{2acos^2\theta + 2bsin^2\theta}$$

In the main text Equation (5), $m_{zz}^* = \frac{\hbar^2}{2a}, m_{ac}^* = \frac{\hbar^2}{2b}$.

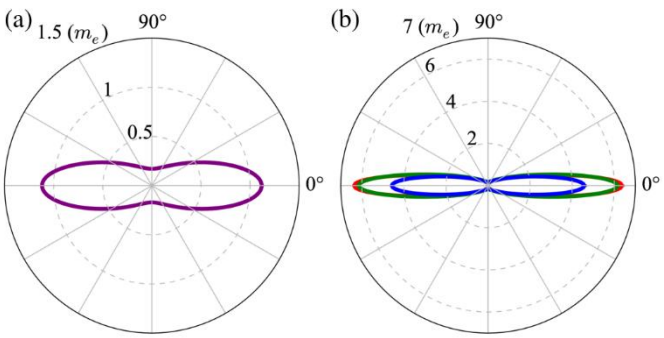

Figure S2. Effective masses based on HSE06 method of (a) electrons and (b) holes in phosphorene under uniaxial stress 0.8 GPa·nm along different directions. For electrons, the effective mass remains nearly unchanged with stress (purple line). For holes, effective mass is sensitive to stress and its direction θ, as shown for

unstressed phosphorene (red), and phosphorene with stress of applied along $\theta = 0°$ (green), and $\theta = 90°$ (blue).

S7. Young's modulus for bulk

Bulk phosphorus is orthotropic materials, its stiffness tensor can be written as:

$$\begin{bmatrix}\sigma_1\\ \sigma_2\\ \sigma_3\\ \sigma_4\\ \sigma_5\\ \sigma_6\end{bmatrix} = \begin{bmatrix}C_{11} & C_{12} & C_{13} & 0 & 0 & 0\\ C_{12} & C_{22} & C_{23} & 0 & 0 & 0\\ C_{13} & C_{23} & C_{33} & 0 & 0 & 0\\ 0 & 0 & 0 & C_{44} & 0 & 0\\ 0 & 0 & 0 & 0 & C_{55} & 0\\ 0 & 0 & 0 & 0 & 0 & C_{66}\end{bmatrix}\begin{bmatrix}\varepsilon_1\\ \varepsilon_2\\ \varepsilon_3\\ \varepsilon_4\\ \varepsilon_5\\ \varepsilon_6\end{bmatrix}$$

Young's modulus along zigzag direction

$$Y_{zz} = \sigma_1/\varepsilon_1$$

$$= \frac{C_{11}C_{22}C_{33} + 2C_{12}C_{23}C_{13} - C_{23}^2C_{11} - C_{13}^2C_{22} - C_{12}^2C_{33}}{C_{22}C_{33} - C_{23}^2}$$

Young's modulus along armchair direction

$$Y_{ac} = \sigma_2/\varepsilon_2$$

$$= \frac{C_{11}C_{22}C_{33} + 2C_{12}C_{23}C_{13} - C_{23}^2C_{11} - C_{13}^2C_{22} - C_{12}^2C_{33}}{C_{11}C_{33} - C_{13}^2}$$

Acknowledgements
The authors thank Dr. Zhili Hu for useful discussions.

Notes and references

[a] Department of Materials Science and Nanoengineering,
[b] Department of Chemistry,
[c] Smalley Institute for Nanoscale Science and Technology, Rice University, Houston, Texas 77005, USA.

* Corresponding author e-mail: biy@rice.edu

1. H. Wang, F. Liu, W. Fu, Z. Fang, W. Zhou and Z. Liu, *Nanoscale*, 2014, **6**, 12250-12272.
2. H. O. H. Churchill and P. Jarillo-Herrero, *Nat Nano*, 2014, **9**, 330-331.
3. L. Li, Y. Yu, G. J. Ye, Q. Ge, X. Ou, H. Wu, D. Feng, X. H. Chen and Y. Zhang, *Nat Nano*, 2014, **9**, 372-377.
4. H. Liu, A. T. Neal, Z. Zhu, Z. Luo, X. Xu, D. Tománek and P. D. Ye, *ACS Nano*, 2014, **8**, 4033-4041.
5. M. Buscema, D. J. Groenendijk, G. A. Steele, H. S. J. van der Zant and A. Castellanos-Gomez, *Nat Commun*, 2014, **5**, 4651.
6. T. Hong, B. Chamlagain, W. Lin, H.-J. Chuang, M. Pan, Z. Zhou and Y.-Q. Xu, *Nanoscale*, 2014, **6**, 8978-8983.
7. Z. Wang, H. Jia, X. Zheng, R. Yang, Z. Wang, G. J. Ye, X. H. Chen, J. Shan and P. X. L. Feng, *Nanoscale*, 2015, **7**, 877-884.
8. F. Xia, H. Wang and Y. Jia, *Nat Commun*, 2014, **5**, 4458.
9. L. Kou, T. Frauenheim and C. Chen, *The Journal of Physical Chemistry Letters*, 2014, **5**, 2675-2681.
10. Z. Zhang, X. Liu, B. I. Yakobson and W. Guo, *Journal of the American Chemical Society*, 2012, **134**, 19326-19329.
11. Z. Zhang, W. Guo and B. I. Yakobson, *Nanoscale*, 2013, **5**, 6381-6387.
12. L. Yuanchang and C. Xiaobin, *2D Materials*, 2014, **1**, 031002.
13. Z. Zhang and W. Guo, *Physical Review B*, 2008, **77**, 075403.
14. Z. Zhang, C. Chen and W. Guo, *Physical Review Letters*, 2009, **103**, 187204.
15. T. Low, R. Roldán, H. Wang, F. Xia, P. Avouris, L. M. Moreno and F. Guinea, *Physical Review Letters*, 2014, **113**, 106802.
16. A. S. Rodin, A. Carvalho and A. H. Castro Neto, *Physical Review Letters*, 2014, **112**, 176801.
17. R. Fei and L. Yang, *Nano Letters*, 2014, **14**, 2884-2889.
18. Q. Ji, Y. Zhang, T. Gao, Y. Zhang, D. Ma, M. Liu, Y. Chen, X. Qiao, P.-H. Tan, M. Kan, J. Feng, Q. Sun and Z. Liu, *Nano Letters*, 2013, **13**, 3870-3877.
19. A. Thean and J. P. Leburton, *Applied Physics Letters*, 2001, **79**, 1030-1032.
20. X. L. Wu and F. S. Xue, *Applied Physics Letters*, 2004, **84**, 2808-2810.
21. L. Seravalli, M. Minelli, P. Frigeri, P. Allegri, V. Avanzini and S. Franchi, *Applied Physics Letters*, 2003, **82**, 2341-2343.
22. S. Mazzucato, D. Nardin, M. Capizzi, A. Polimeni, A. Frova, L. Seravalli and S. Franchi, *Materials Science and Engineering: C*, 2005, **25**, 830-834.
23. Y. G. Wang, Q. L. Zhang, T. H. Wang, W. Han and S. X. Zhou, *Journal of Physics D: Applied Physics*, 2011, **44**, 125301.
24. G. Kresse and J. Furthmüller, *Physical Review B*, 1996, **54**, 11169-11186.
25. J. Heyd, G. E. Scuseria and M. Ernzerhof, *The Journal of Chemical Physics*, 2003, **118**, 8207-8215.
26. J. Heyd, G. E. Scuseria and M. Ernzerhof, *The Journal of Chemical Physics*, 2006, **124**, 219906.
27. J. Qiao, X. Kong, Z.-X. Hu, F. Yang and W. Ji, *Nat Commun*, 2014, **5**, 4475.
28. X. Peng, Q. Wei and A. Copple, *Physical Review B*, 2014, **90**, 085402.
29. Q. Wei and X. Peng, *Applied Physics Letters*, 2014, **104**, 251915.
30. Y. Liu, F. Xu, Z. Zhang, E. S. Penev and B. I. Yakobson, *Nano Letters*, 2014, **14**, 6782–6786.
31. V. Tran, R. Soklaski, Y. Liang and L. Yang, *Physical Review B*, 2014, **89**, 235319.
32. L. Wang, A. Kutana and B. I. Yakobson, *Annalen der Physik*, 2014, **526**, L7-L12.
33. P. Lu, X. Wu, W. Guo and X. C. Zeng, *Physical Chemistry Chemical Physics*, 2012, **14**, 13035-13040.
34. Y. Liu and B. I. Yakobson, *Nano Letters*, 2010, **10**, 2178-2183.
35. G. Qin, Q.-B. Yan, Z. Qin, S.-Y. Yue, H.-J. Cui, Q.-R. Zheng and G. Su, *Sci. Rep.*, 2014, **4**, 6946.